

Performance of a Vacuum Formed Chopped Ceramic Fiber Filter in a Reducing Environment

Rajesh K. Ahluwalia (walia@anl.gov; 630-252-5979)

Vincent J. Novick (vnovick@anl.gov; 630-252-6629)

L. Zhang (fzhang@anl.gov; 630-252-6389)

Manish P. Sutaria (manish_sutaria@qmgate.anl.gov; 630-252-5115)

Jitendra P. Singh (jp_singh@qmgate.anl.gov; 630-252-5123)

Argonne National Laboratory

9700 South Cass Avenue

Argonne, IL 60439-4841

ABSTRACT

A laboratory-scale apparatus has been used for unattended, long duration, continuous, flow-through testing of a vacuum formed chopped ceramic fiber filter under reducing conditions. Four candle specimens were exposed from 150 to 3550 h to 600°C gas containing 4% CO, 11% H₂, 12% CO₂, 14% H₂O, 59% N₂, 1 ppmv NaCl, 50 ppmv H₂S and 1000-2000 ppmw ash from a transport reactor operated in gasification mode. A data base was established on pressure drop of the as-received and exposed filter as a function of face velocity and temperature. Tests were conducted to investigate the effects of back pulse parameters on filter regenerability. Results are reported on the critical reservoir pressure and pulse duration for maintaining a stable saw-tooth profile of pressure drop across the filter element. Data are obtained to characterize the effect of chemical and thermal aging on the apparent bulk density of the filter, pore size distribution, fast fracture strength and microstructure. It is suggested that the compliant filter undergoes a slow process of rigidization upon exposure to the test environment.

INTRODUCTION

Vacuum formed chopped ceramic fiber (VFCCF) filters made by Industrial Filter and Pump Manufacturing Company are being considered for high-temperature particulate removal applications in pressurized fluidized bed (PFBC) and integrated gasification combined cycle plants (IGCC). Compared to isostatically pressed silicon carbide filters, VFCCF candles (trade name Fibrosic) have stated advantages of lightweight construction, stable ceramic oxide materials, high temperature capability, shock and cracking resistance, and ease of surface treatment [1]. At 0.27-0.34 g/cc apparent density, VFCCF candles are 70-80% lighter than their SiC counterparts. The resulting weight saving translates into reduced stress on the flange of the candle filter and simplification of the design and construction of the tubesheet and supporting hardware. The fibers and binders are a blend of stable, pure ceramic oxides, primarily alumina and aluminosilicate materials rated for a maximum use temperature of 1400-1500°C. They do not exhibit significant physical changes, such as shrinkage, until a temperature of about 1260°C. The differences in the thermochemical properties between the binder and fiber are negligible because they are identical in composition. This results in

excellent thermal shock and thermal spalling resistance, as well as resistance to microcracking caused by differences in the thermal expansion coefficients of the fiber and binder. Due to the knitting tendency of the fibers during fabrication, VFCCF candle filters have an inherently high crack resistance. The random orientation of the fibers tends to blunt microcrack propagation. Finally, VFCCF candle filters can be treated with colloidal oxide materials to increase strength, add corrosion resistance and control particle retention.

The purpose of this work was to study the filtration behavior, evaluate regenerability, and assess the effects of extended thermal and chemical aging (more than 2000 h) on the microstructure and thermomechanical properties of the VFCCF filter. All tests were done under controlled reducing conditions in a laboratory setting. Previously, VFCCF candles have been tested under oxidizing conditions in a small PFBC facility at Argonne National Laboratory [2]. In two short-duration tests (exposure time less than 10 h) at 800°C, 9.2 bar and 5.1-10.2 cm/s face velocity, the candles demonstrated excellent resistance to thermal shock imposed by periodic back pulsing with N₂ gas. In both tests, the measured collection efficiency was better than 99.97% corresponding to a mean diameter of 11 μm for particles captured on the filter. In a longer duration test under oxidizing conditions at Tidd (2815 h exposure time), the VFCCF filters were reported to have suffered from thermal fatigue, ruptured in a steam-air environment and rigidized in an alkali-steam-air environment. The filter morphology was not affected by exposure. VFCCF candle filters have also been exposed to a reducing gas from a pilot-scale transport reactor [4]. The test conditions were 475°C temperature, 8.3 bar pressure, 6700 ppm particulate loading and 1.4 cm/s filter face velocity. In 126 h exposure time, the filter was subjected to 70 back pulses of 0.25 s duration and 11.45 bar pressure. The particle size distribution had a median of 11.3 μm upstream and 2.3 μm downstream of the filter. The candles were reported to have ruptured due to penetration of carbon that burnt in-situ when the filter vessel was heated under oxidizing conditions. In-situ combustion of carbon could raise the filter temperature to 800-900°C [5].

EXPERIMENTAL

Figure 1 presents the schematic of the experimental apparatus designed to supply various gases, alkali and fly ash simulating PFBC or IGCC environments and to challenge a filter at temperatures around 600°C. A flanged mulite ceramic tube, 3.75" in diameter x 42" long, is used as the primary confinement vessel for the filters tested in the facility. A second smaller ceramic tube 3.25" in diameter and 30" long, is concentrically mounted inside the first. The inner tube holds and positions the test filter in the tube furnace. A stainless steel flange, modified to mount the back pulse filter cleaning mechanism, provides a seal to the top of the outer ceramic tube. At the bottom of the outer tube, the flange of the inner tube and a stainless steel 3" tee are sealed together with the bottom flange of the outer tube. The outer tube is supported from the bottom flange and is positioned inside a 6" diameter x 36" long, three-zone tube furnace. The furnace provides the mechanism for heating the gases and the filter.

The gases used to simulate the oxidizing and reducing environments are supplied to the branch of the tee below the furnace. Attached to the 3" tee is a reducing union and a 4" tee. Blank flanges on the stainless tees, modified for various feedthroughs, complete the experimental containment. Below the bottom tee is the ash feeder assembly. All gas lines except the ash feed, are

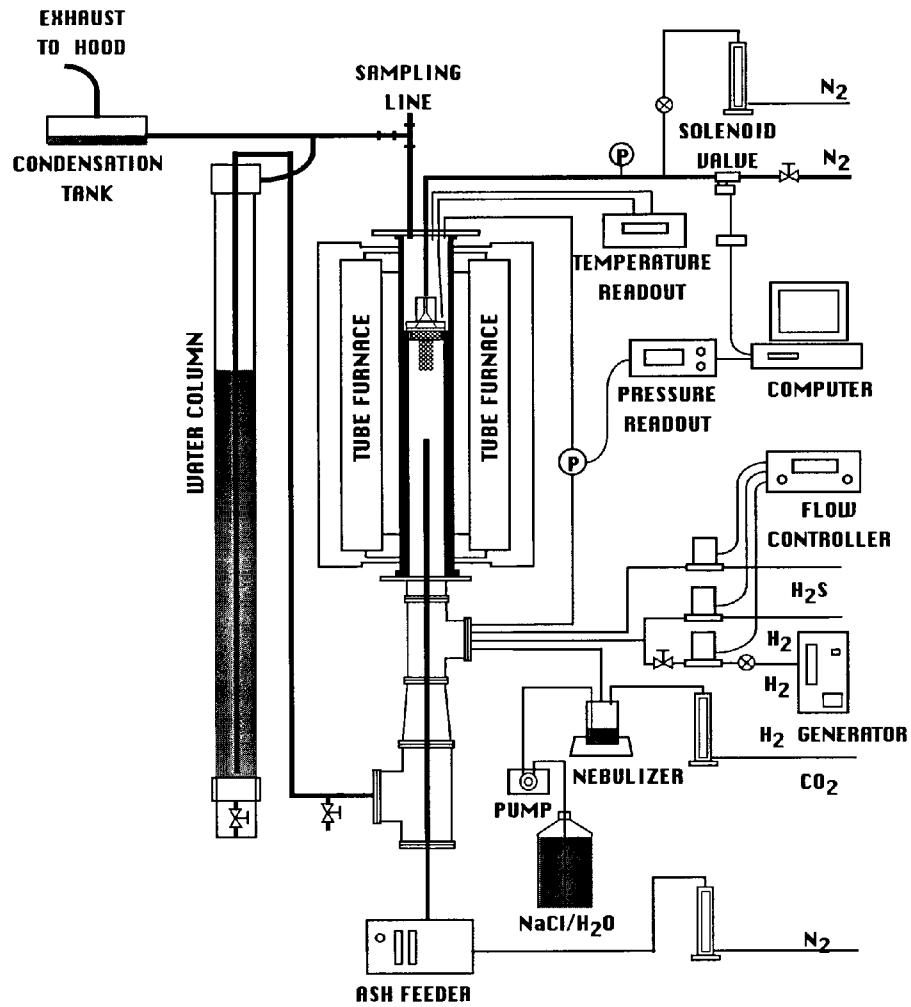


Figure 1. Filter test apparatus.

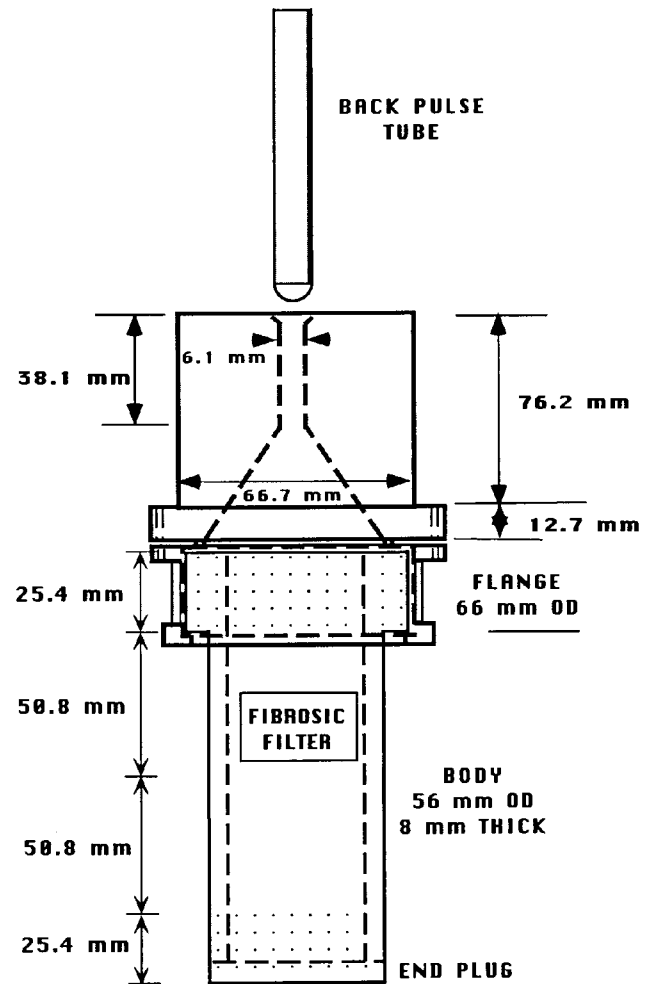


Figure 2. Filter holder and back pulse system.

heat traced to over 100°C, as are the two stainless tees and reducing union. Pure gases, such as N₂ and CO₂, are supplied by pressurized gas cylinders and their flow is controlled through rotameters. Hydrogen is supplied by an electrolytic generator with an output capacity of 1.2 lpm. Additional hydrogen is supplied by a pressurized gas cylinder, if necessary. The H₂ is regulated with mass flow controllers. Water vapor is supplied by nebulizing water into droplets which are carried by the CO₂. The nebulizer is supplied by a peristaltic pump and a four-liter reservoir of distilled water. The alkali challenge to the filter is in the form of sodium chloride, which is added to the water before nebulization. Control of the amount of water vapor and alkali supplied to the experiment is provided by the flow rate of CO₂, the nebulizer power setting, the peristaltic pump setting and the concentration of NaCl in the feed solution.

The N₂ gas added to the test environment also provides for the dispersion of the ash into an aerosol and its transport into the containment tube. The ash is regulated by a chain drive mechanism that transports it from a powder reservoir to the dispersal position using the adhesion of the ash onto the beads of the chain. The ash is blown off the bead by a jet of N₂ gas. The concentration of the aerosolized fly ash is determined by the speed of the chain supplying the ash and the volume flow of N₂ gas. The aerosolized fly ash is conveyed to the test filter through a long vertical 1/4" ceramic tube. The tube allows the N₂ carrier gas to maintain sufficient velocity to keep the fly ash suspended until the N₂ gas becomes hot enough so that, upon expansion in the 3 1/4" ceramic tube, the gas continues to carry the particles to the filter. Ash that is removed from the filter during the back pulse process falls to the bottom of the 4" tee at the base of the apparatus. The falling ash cannot reenter the ash supply tube because of the high velocity of gas in the 1/4" tube. Re-entrainment of the ash is minimized by allowing the back pulse of gas to flow out of the 3" tee below the furnace and through a water column, to the exhaust line. This keeps the removed ash entrained in the back pulse gas until it reaches the cooler region outside the furnace where the upward flow is insufficient to suspend the fly ash. The water column also provides a safety mechanism to automatically release pressure from containment if it exceeds the height of the water. This feature can protect equipment in a scenario where the filter blinds during unattended operation.

Pressure data is acquired every two seconds on a Mac Iix personal computer. A program was written to automatically acquire data, pulse the filter with back flow gas on a pressure limit or timed schedule and to write one day's worth of data to a file for archiving. The ΔP across the filter is measured with a capacitance manometer, with an accuracy of better than 0.25 torr. The computer also controls the frequency, duration and multiples of the back pulse of cold gas to the filter for cleaning purposes.

A schematic of the back pulse tube, filter holder and filter geometry is given in Fig. 2. The back pulse tube, with an outlet orifice of 1.2 mm, is positioned approximately 3 mm above the filter holder. The filter holder consists of two pieces, one is designed to distribute the back pulse gas over the entire cross sectional area of the filter, while the other is designed to clamp the ceramic filter to the distributor. Both pieces are made of inconel for corrosion resistance. The distance between the back pulse tube and the filter holder is critical to the operation and interpretation of the test results. If the tube is too close, a significant pressure drop can be created by the narrow gap and will be added to the overall ΔP measured by the capacitance manometer. If the tube is too far from the holder, a fraction of the back pulse gas will not enter the distributor and not contribute to the filter's

regeneration. The typical procedure was to find the minimum distance from the holder that did not contribute to an increase in ΔP as measured by the pressure transducer.

However, in some of the tests, a rapidly increasing ΔP that could not be recovered by back pulsing the filter, was found to be related to the positioning of the back pulse tube and not to the blinding of the filter. It is suspected that either some type of corrosion or unfiltered ash caused a bridge across the narrow gap between the tube and holder which resulted in the observed increase in ΔP . Sometimes readjusting the position of the tube resolved the problem, other times the test had to be terminated. For the Filter 3 test, the experiment was shut down, the apparatus was cleaned and the test was restarted. It was determined that a small (nominally 0.5 lpm) of N_2 gas at low pressure, continuously admitted through the back pulse tube, eliminated the phenomenon. Conclusions as to the cause of the phenomenon could not be reached because the design of the filter holder and back pulse tube did not allow for their removal as a single unit for visual inspection.

The gas composition used in the tests was intended to be representative of a gasifier environment at atmospheric pressure. It was assumed that a desulfurization unit upstream of the filter could reduce H_2S concentration to less than 200 ppmv. Table 1 lists the target composition of the feed. For safety reasons, the input gas did not contain CO. Instead, the water-gas shift reaction was relied upon to produce CO through reduction of CO_2 in the chamber. During the test campaign, significant condensation of water vapor was noted in the cooler regions of the ash collection tee at the bottom of the assembly. To prevent unseen problems later in the campaign, H_2O feed rate was reduced below the target value. Some difficulty was experienced early on in regenerating the Fibrosic filter. Late in the campaign, it was realized that the difficulty was at least partly related to the incorrect positioning of the back pulse tube relative to the venturi. To enhance the probability of running a successful long-duration test, the H_2S concentration too was lowered below the target value. Based on the experience gained from the tests, it is believed that both steps were unnecessary. Note that the quantity of ash challenging the filter was limited by the beaded chain supply mechanism of the ash feeder.

The ash used to challenge the filters in this test, came from the Transport Reactor Demonstration Unit Run number PO47. Table 2 lists the composition of the ash analyzed using X-ray fluorescence and X-ray diffraction. Air was used as the dispersion gas to aerosolize ash into standard atmospheric conditions. The ash was stored in a laboratory furnace at about $110^\circ C$ for at least one day before placing it in the generator for dispersal. The intent was to improve aerosolization by removing moisture that might cause the ash to adhere strongly and impede efficient dispersal. The particle size distribution measurements were made with an eight-stage cascade impactor, with cut points ranging from $0.3 \mu m$ to $10 \mu m$. The measured size distribution was graphed as a log-probability plot and the mass median aerodynamic diameter (MMAD) of the dispersed ash was extrapolated to be $15.6 \mu m$.

Figure 2 also presents the schematic of the Fibrosic filters tested. The mean fiber diameter is specified as $3 \mu m$ and the mean binder particle diameter as 20 nm. The supplier impregnates the clean and dirty sides of the filter element with alumina to “normalize” the pore size and to toughen the skin. A filter specimen is 152 mm long, 8 mm thick, and has nominal outer diameter (OD) of

Table 1. Composition of gas used in the exposure tests. The feed column denotes the amount of gas supplied. The equilibrium column is calculated based on stoichiometry and gas phase reactions.

	Target feed	Target equilibrium	Filter 1 avg feed	Filter 2 avg feed	Filter 3 avg feed	Filter 4 avg feed
CO	0	4.3%	0	0	0	0
H ₂	15%	10.7%	15.1%	13.8%	13/5%	15.3%
CO ₂	16%	11.7%	16.1%	15.4%	14.8%	14.3%
N ₂	59%	59%	60%	65.4%	66.1%	64.8%
H ₂ S	200 ppm	200 ppm	75 ppm	21 ppm	31 ppm	32 ppm
H ₂ O	10%	14.3%	8.8%	5.4%	5.6%	5.6%
NaCl	1 ppm	1 ppm	none	1.14 ppmv	0.891 ppmv	1.38 ppmv
Ash	2000 ppmv	2000 ppmv	1265 ppmv	1847 ppmv	1285 ppmv	1625 ppmv
Exposure time			148 h	307 h	3532 h	263.3 h
No. of cleaning pulses			535	612	8353	1165
Temperature	600°C	600°C	600°C	600°C	600°C	588°C
Pressure	1 atm	1 atm	1 atm	1 atm	1 atm	1 atm

56 mm. It has a flange, 66 mm in OD and 25.4 mm in length. The flange is treated post fabrication to triple its density and increase its strength. Portions of the filter bottom (25.4 mm) and the body (50.8 mm) adjacent to the flange are rendered impervious by the same densification process. Thus, only 50.8 cm of the body is permeable to flow giving a net filtration area of 89.37 cm². The test specimen was sealed to the filter holder with a flexible ceramic fiber felt mat, sandwiched between the filter and the collar and diverter holder assemblies. The assembled filter holder was then sealed to the inner ceramic tube with more of the ceramic fiber felt mat, using the weight of the filter holder assembly to provide sufficient compression of the mat. This sealing mechanism was shown to be adequate, based on a comparison of ΔP measurements as a function of flow rate between a neoprene rubber sealing fixture and the mechanism described previously. To within the limits of the capacitance manometer, the ΔP measurements at each flow rate were identical with both sealing techniques. This implies that there is no significant leakage around the ceramic mat seal.

Table 2. TRDU ash analysis

Oxides	Wt%	Elemental	Wt%
SiO ₂	50.4	Si	46.6
Al ₂ O ₃	20.1	Al	21.7
Fe ₂ O ₃	1.4	Fe	2.0
TiO ₂	0.7	Ti	0.9
P ₂ O ₅	0.8	P	0.7
CaO	12.8	Ca	18.1
MgO	6.9	Mg	8.3
Na ₂ O	0.7	Na	1.1
K ₂ O	0	K	0
SO ₃	1.1	S	0.8

FILTER PERFORMANCE

Pressure Drop Behavior

A parametric study was conducted on Filter 4 to determine the relationship between ΔP , gas flow rate, temperature and the condition of the filter. Figure 3 presents the data from a series of experiments in which ΔP was measured as a function of N₂ flow rate and furnace temperature. The open symbols represent the clean filter data. The pressure drop is observed to increase with gas temperature because of higher face velocity and gas viscosity. The filled symbols represent the data from the exposed filter. The variability in pressure drop data at 600°C (filled circles) for a given flow rate reflects the effects of repeated back pulses of N₂ gas, pulse durations, reservoir pressures and the time between pulses. The data for 500°C (filled squares) is representative of the day-to-day variation in pressure drop as a function of flow rate. The difference between ΔP of the exposed and clean filter for identical temperature and flow rate is a measure of the additional resistance to gas flow offered by the layer of adherent ash that builds up over numerous cleaning cycles.

The pressure drop data can be reduced by calculating the effective permeability or permeance (k_{eff}) from the Darcy-Forchheimer equation.

$$k_{\text{eff}} = \frac{\mu v(1+\text{Re})}{\Delta P} \quad (1)$$

$$\text{Re} = \frac{\beta \rho v}{\mu} \quad (2)$$

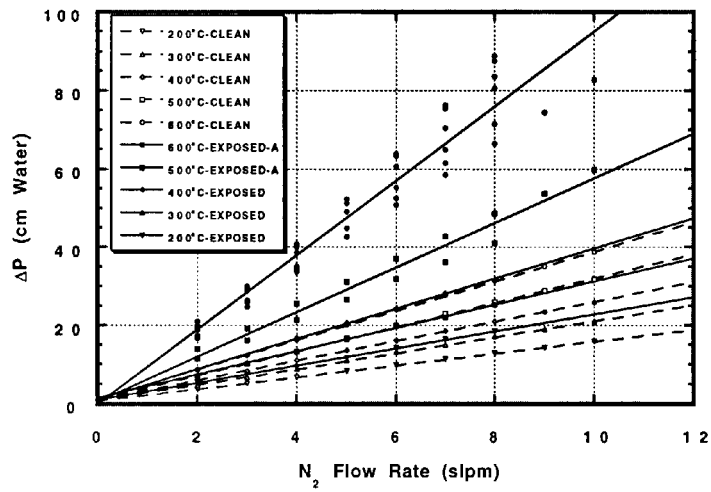


Figure 3. Filter 4 pressure drop behavior as a function of gas flow rate and temperature for both clean and exposed conditions.

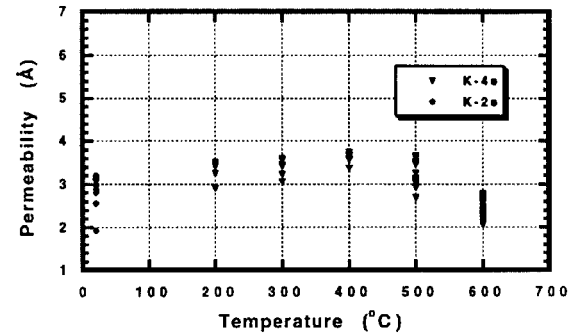
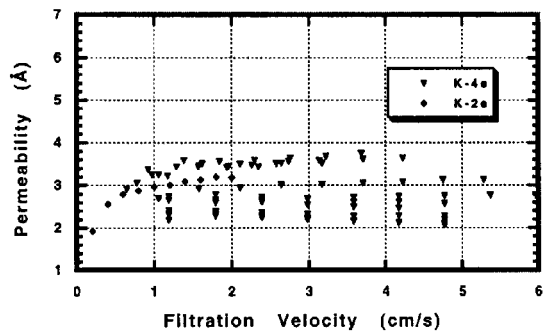
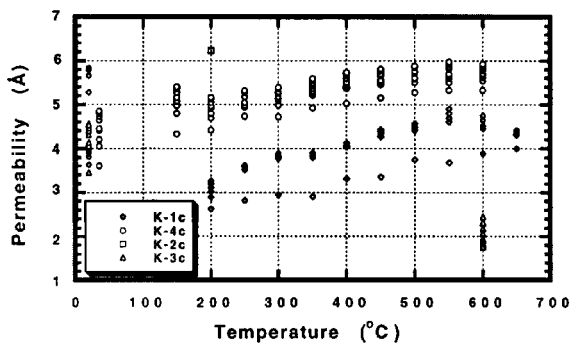
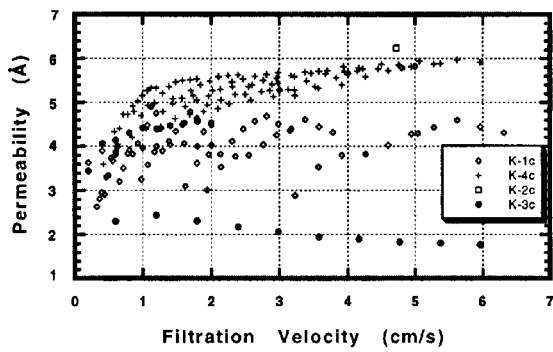


Figure 4a. Derived permeability as a function of filter face velocity for both clean (upper) and exposed (lower) conditions.

Figure 4b. Derived permeability as a function of temperature for both clean (upper) and exposed (lower) conditions.

where ρ is the gas density, μ is the gas viscosity, v is the face velocity and β is an empirical coefficient to account for inertial effects. With $\beta = 0$ and data for all combinations of temperature and flow rate included, an average k_{eff} of $4.05 \pm 0.63 \text{ \AA}$ is inferred for clean Filter 4. The error bar is somewhat larger for Filter 1 because the data for 1 slpm was included. The pressure drop at this flow rate was always inconsistent. Disregarding 1 slpm data, the average k_{eff} for Filter 1 becomes $4.17 \pm 0.58 \text{ \AA}$. Figure 4 plots the effective permeability as a function of N_2 gas temperature and velocity. There is a visible trend of k_{eff} increasing with gas temperature and face velocity. At a given temperature, the variability in k_{eff} is due to different face velocities. Similarly, the variability in k_{eff} at a constant face velocity is due to differences in gas temperature. The pressure drop data can be reduced better by including the inertial effects in Eq. (1). The filter to filter variation in k_{eff} , however, is even larger even though they came from the same manufactured lot. Note that the filtration area was calculated and assumed to be the same for different specimens. However, the potential difference in filtration area is not expected to account for the observed variation in k_{eff} between the filters.

The pressure drops for Filters 2 and 4 were measured as a function of N_2 gas flow rate and temperature during the cool-down phase of the exposure tests summarized in Table 1. The average effective permeability for Filter 2 at 20°C is $2.88 \pm 0.39 \text{ \AA}$. For Filter 4, the average k_{eff} over the temperature range 20°C - 600°C is $2.86 \pm 0.52 \text{ \AA}$. One effect of exposure to ash is to reduce the filter-to-filter variation in k_{eff} measured with the as-received specimens. On exposure, the effective permeability reduces because of the ash cake that forms on the outer surface and possible penetration of ash into the interstices of the filter. The contribution of ash to k_{eff} can be deduced by representing it as two resistances in series.

$$\frac{1}{k_{\text{eff}}} = \frac{1}{k_{\text{eff}}^{\text{o}}} + \frac{1}{k_{\text{eff}}^{\text{ash}}} \quad (3)$$

The data suggests that for filters from the same manufactured lot challenged by same ash at identical operating conditions, $k_{\text{eff}}^{\text{ash}}$ is apparently inversely proportional to the effective permeability of the virgin specimen, $k_{\text{eff}}^{\text{o}}$. For Filter 4, $k_{\text{eff}}^{\text{ash}}$ is estimated as $6.31 \pm 0.96 \text{ \AA}$. Post-test examination of one of the exposed filters revealed nearly uniform coating of the residual ash and a cake thickness of 0.5-1 mm.

Figure 4 also depicts the dependence of the k_{eff} for the exposed filters on gas temperature and face velocity. The effective permeability appears to increase with temperature over the range 20 - 400°C . Whereas k_{eff} for the clean filter becomes flat above 500°C or slightly decreases, it clearly decreases with temperature above 400°C for the exposed filters. Also, the effective permeability for the exposed filters is relatively constant for face velocity exceeding 1 cm/s .

Filter Collection Efficiency

The particle collection efficiency of the Fibrosic filter was measured at 1435 h into the 3530 h exposure test of Filter 3. A cascade impactor was installed in the exhaust line directly above the outlet of the filter holder assembly. The amount collected by the stages of the cascade impactor was compared to mass distribution of the fly ash as dispersed in separate off-line tests of the ash feeder. In addition, the total mass output per unit time of the ash feeder was measured. The average mass

median aerodynamic diameter (MMAD) of the particulates aerosolized by the ash feeder was 15.6 μm . The average output of the ash feeder was 8.15 mg/min with an aerosolization efficiency of 45.8%. A total of 0.29 mg of ash was collected after 6 h of sampling at 1 slpm downstream of the filter. Analysis of the cascade impactor and ash feeder data show that 99.96% of particles larger than 16 μm , 99.83% of particles between 7.85 μm and 16 μm , 99.86% of particles between 4.24 μm and 7.85 μm , 99.89% of particles between 2.05 μm and 4.25 μm , and 99.92% of particles between 1.09 μm and 2.05 μm were collected by the filter. The total collection efficiency based on the mass collected downstream of the filter and the estimated mass challenging the filter was determined to be 99.92%.

Filter Loading and Cleaning Behavior

A test sequence was designed to explore if any one constituent of the environment caused an unreasonable increase in ΔP across Filter 1 or problems with filter regeneration. Starting with pure N_2 and a furnace temperature of 200°C, each constituent was added and the filter behavior was followed for up to 24 h. With pure N_2 and 200°C furnace temperature, a pressure drop of 31 cm H_2O was noted at 4 cm/s face velocity. Ash was added and the cleaning schedule was set as a double pulse of 200 ms duration and 0.5 s apart, every 20 min from a N_2 reservoir at 9.5 bar. Over 4 h, a saw-tooth profile developed with baseline ΔP gradually increasing and stabilizing at 58 cm H_2O . A series of 10 pulses over a 6 min period from a N_2 tank at 11.2 bar lowered the baseline ΔP to 51 cm H_2O . Additional 15 pulses over the same period further decreased the baseline ΔP to 48 cm H_2O . Over the next 4 h, it was demonstrated that a stable saw-tooth ΔP profile could be maintained with a single pulse of 0.5 or 1 s duration and a reservoir pressure of 11.2 bar. The stable baseline ΔP was 51-52 cm and the increment in ΔP was 2 cm between consecutive pulses with 20 min interval.

The furnace temperature was raised in increments of 100°C, N_2 flow was adjusted to maintain relatively constant filtration velocity, and ΔP was monitored for 24 h at each temperature setting. No deviations from the stable loading and regeneration cycle were noted. The additions of CO_2 , H_2 and H_2O did not affect the cycle, nor did the addition of alkali. Admission of H_2S appeared to increase the pressure drop. On turning off H_2S flow, it took about 24 h for the baseline ΔP to reach the original level prior to addition of H_2S .

Tests with Filter 4 were dedicated to investigating the effects of back pulse parameters on the effectiveness of filter regeneration at 500°C and 600°C. Figure 5 presents the data on the effect of reservoir pressure on ΔP profile. At 600°C furnace temperature, 1 s pulse duration and 60 min pulse interval, a stable repetitive saw-tooth profile is established at 11.2 bar reservoir pressure. Under the same conditions, a saw-tooth profile is also evident at 7.8 bar reservoir pressure but it is non-repetitive because of the creep in baseline ΔP . There is only a partial recovery in ΔP with each back pulse so that the pressure drop rises from one pulse cycle to the next. A saw-tooth profile is not observed at 4.4 bar reservoir pressure. At this operating condition, the back pulse is ineffective in regenerating the filter and there is little or no recovery in pressure drop. Thus, the three reservoir pressure levels can be associated with the limiting conditions of complete, partial and zero recovery of ΔP with back pulsing.

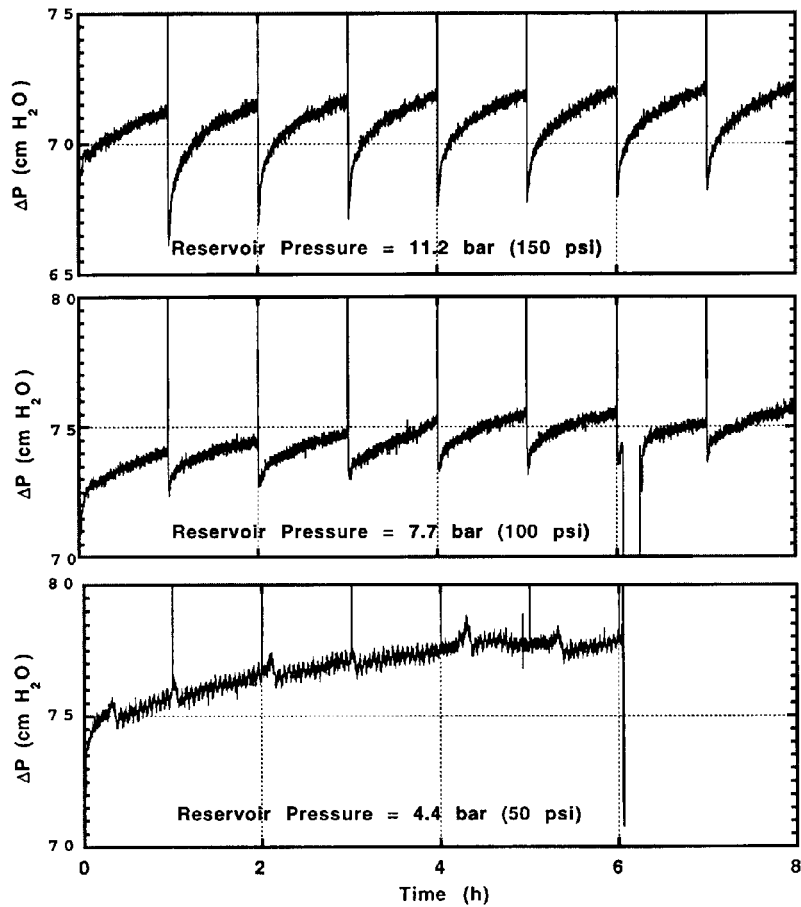


Figure 5a. Measured ΔP across the filter as a function of time, showing the effect of the back pulse reservoir pressure on the effective cleanability of the filter for a 1 s pulse duration and a temperature of 600°C.

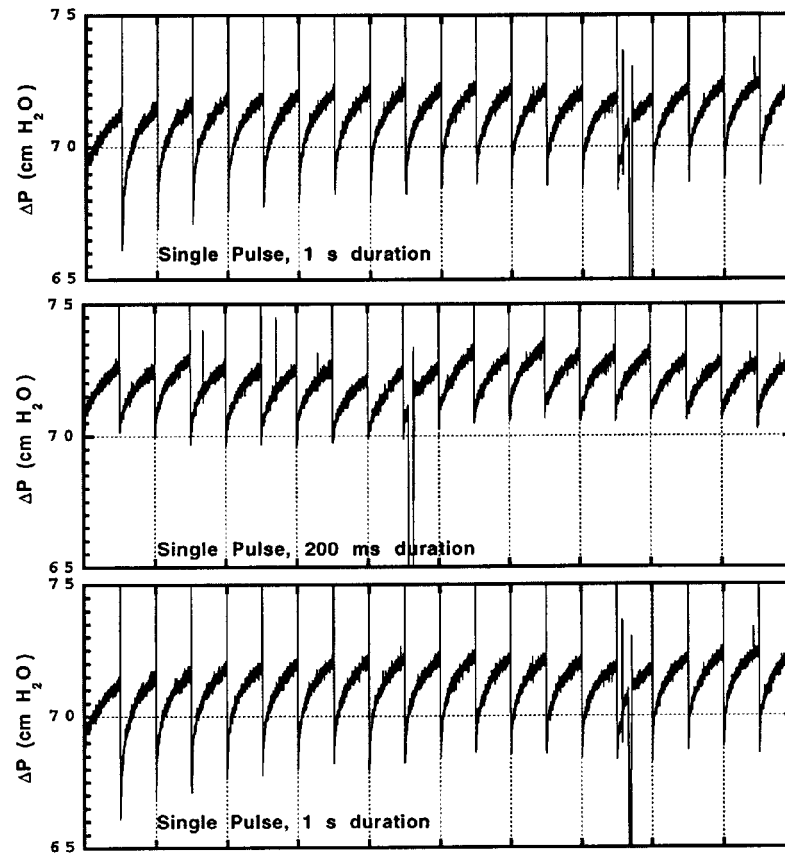


Figure 5b. Measured ΔP across the filter as a function of time, showing the effect of the back pulse duration on the effective cleanability of the filter at a reservoir pressure of 11.2 bar and a temperature of 600°C.

Figure 5 also compares data on filter regenerability as a function of pulse duration and frequency at 600°C furnace temperature and 11.2 bar reservoir pressure. The data shows that a pulse duration of 200 ms is sufficient to repetitively regenerate the filter. The baseline pressure is somewhat lower with 1 s pulse duration but the gas consumption is five times as large. A stable saw-tooth profile can also be established with a double pulse, 100 ms in duration and 500 ms apart. However, a double pulse does not appear to offer any advantages over a single pulse of the same total duration.

Tests were also run to examine the effect of pulse interval on filter regenerability. At 600°C, 11.2 bar reservoir pressure and 1 s pulse duration, the differences in ΔP traces between 20-min, 60-min and 120-min pulse interval tests were considered insignificant. In each case, ΔP profiles were repetitive, the baseline pressures were similar, and the increase in pressure drop between pulses was proportional to the time interval.

The above results suggest that there is a critical reservoir pressure below which the VFCCF candle cannot be regenerated by the simple back pulse technique. Above this critical pressure, a short pulse is as effective in maintaining a stable saw-tooth profile as a long pulse although the baseline pressure is affected by pulse duration. Pulse schedule, single or multiple pulses and interval between pulses, does not appear to significantly impact filter regenerability. For the solenoid valve used in the test apparatus, 18-ms opening and 30-ms closing time, 200-ms pulse duration was adequate to regenerate the filter. At 11.2 bar reservoir pressure, the required specific flow rate of the pulse gas is 1.35 slpm/cm² of filtration area. Thus, the projected compressed gas consumption for a standard 1500-mm long, 60-mm OD candle is 12.7 sl/pulse/filter at 200-ms pulse duration.

MECHANICAL PROPERTIES

The four Fibrosic filters exposed to the reducing conditions were examined for changes in physical properties, mechanical properties and microstructure. Two virgin candle filters were obtained to establish the reference properties. These were identical to the filters that were exposed in that they came from the same production lot number. The virgin filters, however, did not have a triple density flange or the end plugs at the opposing ends. They had the same inner diameter, 39.4 mm, but somewhat larger outer diameter, 60 mm. The filters exposed to the tests were actually machined down to 55.4 mm OD from 60 mm OD in order to fit the experimental apparatus.

Physical Properties

The apparent density of the filter material was measured by a geometrical method. Rectangular specimens were cut by a diamond saw and ground to remove surface roughness. The apparent bulk density, calculated from the measured mass and volume of the rectangular specimens, is listed in Table 3. A bulk density of 0.293 g/cm³ was measured for the virgin filter. The bulk density was observed to increase with exposure; the average density of the four exposed filter specimens was 0.374 ± 0.037 g/cm³. The phenomenon of increase in apparent bulk density with exposure to ash, steam, alkali and H₂S in a reducing environment was confirmed with data from mercury intrusion porosimetry.

Table 3. Physical and mechanical properties of Fibrosic candle filters. Filter 0 is the virgin specimen.

	Filter 0	Filter 1	Filter 4	Filter 2	Filter 3
Exposure Time, h	0	148	243	307	3532
Bulk Density, g/cm ³ (Geometrical Method)	0.293	0.325	0.413	0.370	0.387
Bulk Density, g/cm ³ (Mercury Intrusion)	0.341	0.400		0.350	0.420
Porosity	0.85 (0.73)	0.68 (0.59)		0.77 (0.66)	0.68 (0.59)
Median Pore Size, μm	40.31	24.31		24.17	23.51
Cumulative Intrusion Volume, cc/g	2.5	2.0		2.25	2.0
Fracture Strength, kPa (O-Ring Compression)	401.30 ± 23.00	843.11 ± 30.00	1533.65 ± 124.75	1741.60 ± 10.75	1819.25 ± 186.15
Flexural Strength, kPa (Three-Point Bending)	515.95 ± 129.98				
Elastic Modulus, kPa	43 \pm 21				

The porosity of the filter materials was measured by mercury intrusion porosimetry. This method also provided bulk density, total open porosity, and the pore size distribution. The bulk density measured with the mercury intrusion porosimetry was 0.341 g/cm³ for the virgin filter and 0.390 \pm 0.036 g/cm³ for the exposed filters. As with apparent bulk density, it increased with the time of exposure.

Figure 6 presents the measured cumulative intrusion volume as a function of pore diameter for the as-received and exposed filters. The virgin filter has a bimodal size distribution with about 15% of the intrusion volume associated with the submicron pores. More than 80% of the intrusion volume is accounted for by pores in the 10-90 μm diameter range. The median pore diameter is 40.3 μm and the cumulative intrusion volume is 2.5 cc/g.

The virgin filter is estimated to have a porosity of 85%. Upon exposure, the cumulative intrusion volume decreased to 2.12 \pm 0.12 cc/g as did the median pore size to 23.91 \pm 0.4 μm . The data suggests that the intrusion volume associated with the submicron pores experienced only a minor change. Much of the decrease in intrusion volume is due to partial closing of the macro pores. It appears that the intrusion volume and the median pore size decrease precipitously (within 150 h) as the filter is exposed to the ash-laden flow. Subsequently, the rate of decrease of intrusion volume/median pore volume appears to slow down.

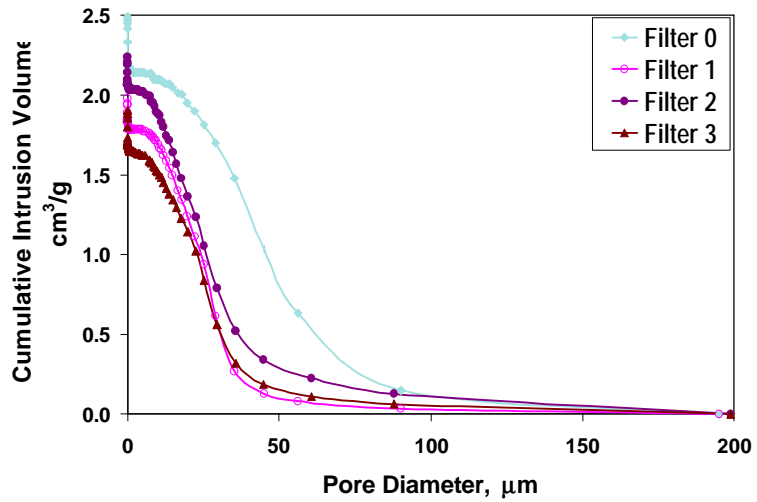


Figure 6. Effect of exposure on pore size distribution represented as cumulative intrusion volume less than stated pore diameter.

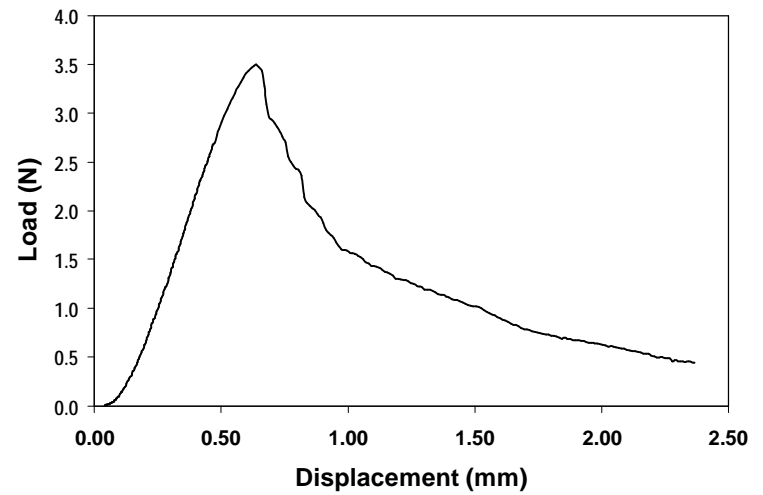


Figure 8. Load-displacement plot from three-point

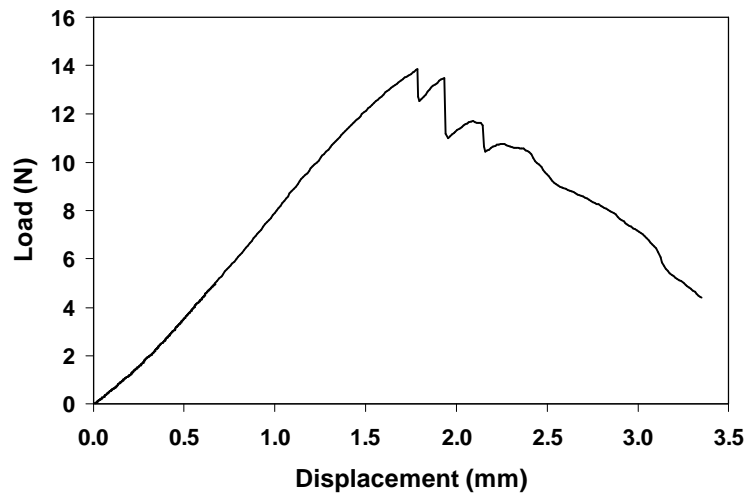
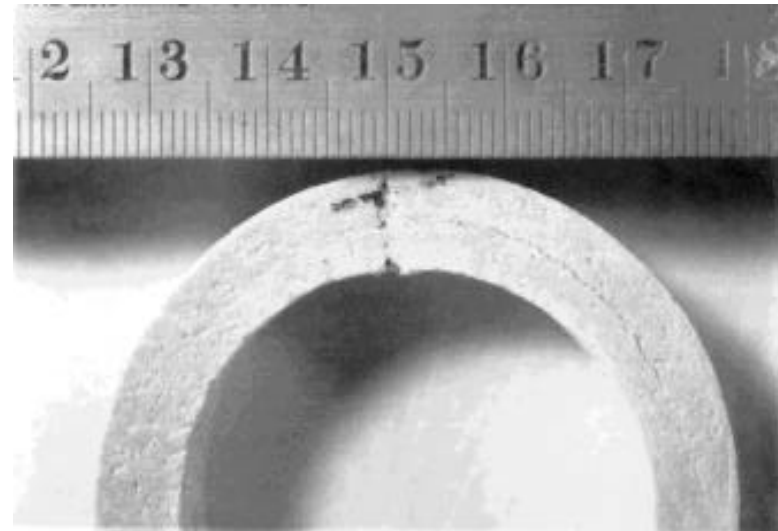


Figure 7. Typical load-displacement plot and failure mode in O-ring compression tests.



Also listed in Table 3 is the filter porosity estimated from the cumulative intrusion volume and the bulk density of the virgin filter. Two estimates are given, one is based on the bulk density deduced from the geometrical method and the other from the mercury intrusion porosimetry. The data indicates that the filter porosity decreases by $14.7 \pm 5.3\%$ due to exposure to ash.

Mechanical Properties

O-Ring Compression Tests. O-ring specimens, 0.5" (1.27 cm) wide, were cut from each candle filter using a diamond saw. Two specimens were tested for each exposed filter and four for the virgin filter. These specimens were loaded to failure in a diametral compression mode on an Instron mechanical testing machine at a cross-head speed of 0.15 cm/min. The maximum stress is developed at the inner diameter across the load points. The fast fracture strength, σ_f , is given by

$$\sigma_f = \frac{PK}{\pi bl} \quad (4)$$

where P is the fracture load, K is a function of the ratio of inner to outer diameters, b is the outer radius of the specimen, and l is the length of the tube. The calculated fracture strength is listed in Table 3.

A typical load-displacement plot of a filter tested in the O-ring compression test is presented in Fig. 7. The plot shows a characteristic composite material behavior. All specimens failed by debonding of the ceramic layers within the filter walls.

The fast fracture strength of the virgin filter was measured to be 401.3 ± 23 kPa. It increased monotonically with time of exposure to the reducing gas containing alkali, H_2S , water vapor and ash. The fracture strength increased to 843.1 ± 30 kPa after 148 h, 1741.6 ± 10.8 kPa after 307 h and 1819.2 ± 186.2 kPa after 3532 h. The limited data suggests that the chopped ceramic fiber filter experiences a rapid improvement in strength for the first 300 h of exposure and a gradual increase thereafter. No degradation in strength was observed within 3500 h of exposure.

Besides fracture stress, there are other indicators of the compliant filter becoming rigidized upon exposure to the reducing gas. In the O-ring compression test, the uncompensated deflection of the specimens at peak load was observed to generally decrease with time of exposure. The measured deflection was 1.49 ± 0.29 mm after 148 h, 0.64 ± 0.03 mm after 243 h, 1.05 ± 0.18 mm after 307 h, and 0.66 ± 0.01 mm after 3589 h. Similarly, the slope of the load-deflection curve, which should be proportional to the elastic modulus, was 16.7 N/mm for the ash-received filter specimen, 9.52 ± 1.32 N/mm after 148 h, 46 ± 0.8 N/mm after 243 h, 27.61 ± 9.81 N/mm after 307 h, and 50.15 ± 4.65 N/mm after 3532 h. More data is required to confirm the increase in stiffness with time of exposure.

Three-Point Bending Tests. Flexural strength was measured on rectangular bar specimens in a three-point bending mode. The specimens were cut by a diamond saw and polished on a 600 grade SiC grinding paper. The final dimensions were 48.25 mm x 8.90 mm x 5.10 mm. A loading span of 38 mm and a cross-head speed of 0.15 cm/min were used for strength measurement. Figure 8 shows a typical load-displacement plot for a filter specimen. The plot depicts a graceful failure

rather than a brittle failure. The flexural strength and the elastic modulus can be calculated using the equations

$$\sigma_f = \frac{3PL}{2bh^2} \quad (5)$$

$$E = \frac{PL^3}{12bh^3y_{\max}} \quad (6)$$

where P is the maximum load, L is the loading span, b is the width of the specimen, h is the height of the specimen, and y_{\max} is the deflection. The average flexural strength for the seven replicate virgin specimens is calculated to be 515.95 ± 129.98 kPa; the average elastic modulus is 43 ± 21 kPa.

Microstructure

Scanning electron microscopy (SEM), coupled with energy-dispersive X-ray (EDX) analysis, was performed on fractured surface (radial cross-section) of filter specimens to investigate penetration of ash particulates and/or chemical reactions. Figure 9 shows a SEM micrograph of the virgin filter. It indicates a composite material with a high volume of fiber content. EDX analysis revealed aluminosilicate peaks for both the fiber and the matrix.

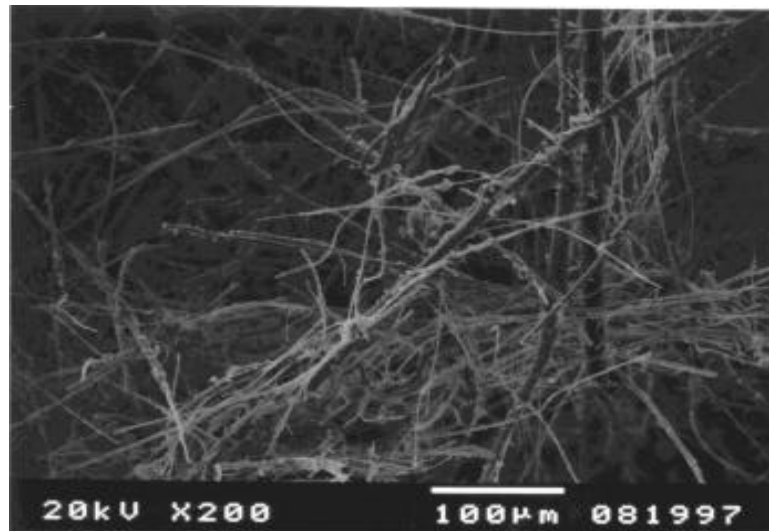


Figure 9. SEM micrograph of virgin filter showing composite material with a high fiber content.

SEM and EDX analyses were performed on the inner and outer surfaces of the cylinder to investigate ash penetration. Figure 10 shows a large amount of debris on both inside and outside layers of Filter 1, indicating significant ash penetration. During the experiment, this filter proved difficult to regenerate by back pulsing. EDX analysis of both fibers and matrix did not show any difference between the inner and outer surfaces. Furthermore, the EDX peaks for this filter were the same as those for the virgin filter. Thus, there was no significant chemical attack during exposure. For Filter 2, there was little evidence of ash particles accumulating on the inside or outside surfaces.

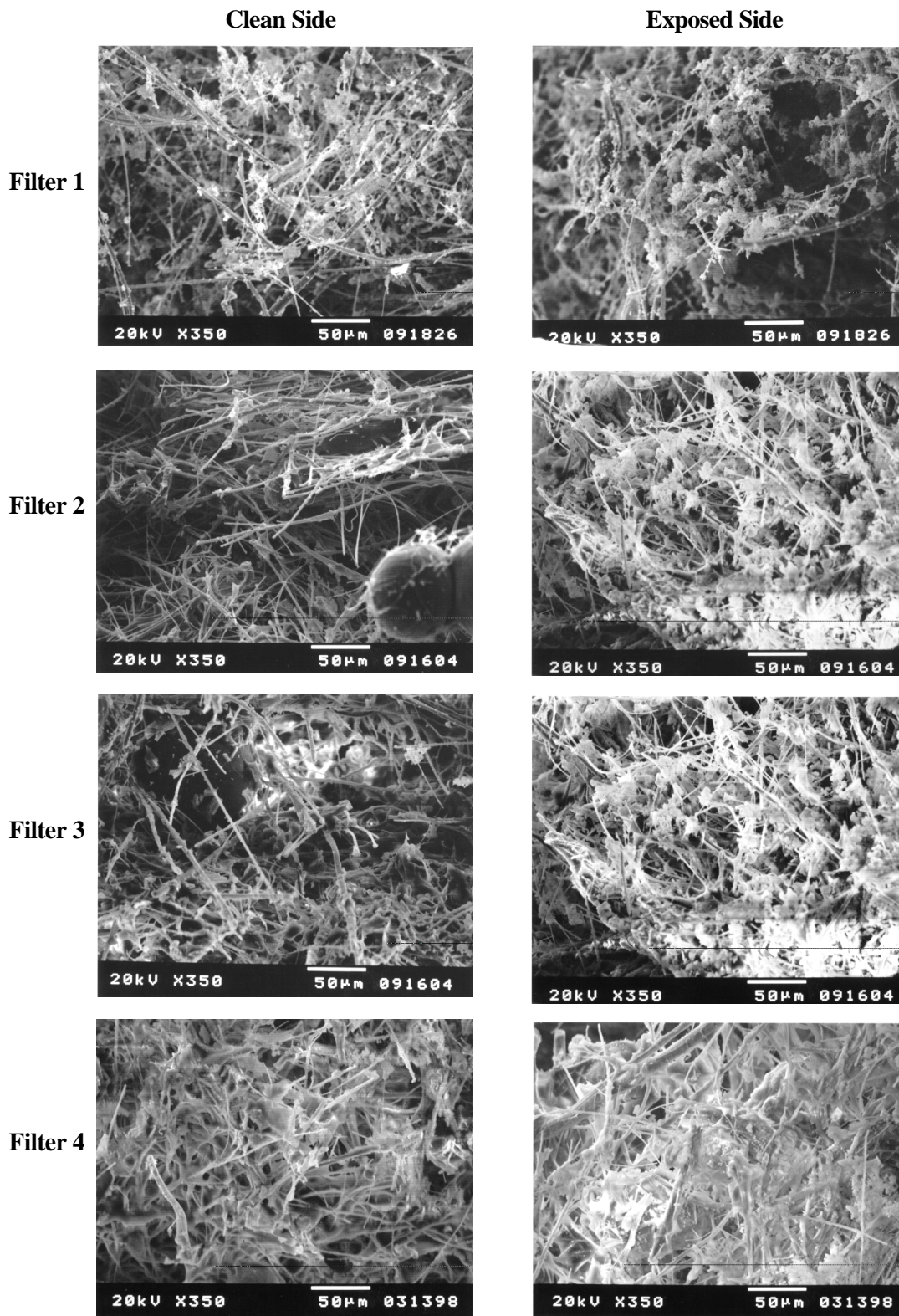


Figure 10. SEM micrographs of clean (inside) and exposed (outside) surfaces of Filters 1, 2, 3 and 4.

For Filter 3, ash particles are visible on the exposed outside surface but not on the inside surface. This is indicative of little ash penetration and an effective regeneration cycle. For Filter 4, ash accumulation on the outside surface is evident with some indication of ash breakthrough to the inner surface.

SUMMARY AND CONCLUSIONS

A laboratory-scale apparatus has been assembled for unattended, long duration, continuous, flow-through testing of advanced, high temperature, particulate filters for application in pressurized fluidized bed combustion and integrated gasification combined cycle plants. It includes a provision for on-line, computer-controlled, back-pulse cleaning of the fouled filter element. The apparatus has been used to test the vacuum formed, chopped ceramic fiber (VFCCF) filter specimens supplied by Industrial Filters & Pump Manufacturing Company. The objectives of the tests were to study the pressure drop behavior, evaluate regenerability, and assess the effects of thermal and chemical ageing on the microstructure and thermomechanical properties of the VFCCF filter. Four specimens were exposed from 150 to 3550 h to a 600°C reducing gas environment containing 4% CO, 11% H₂, 12% CO₂, 14% H₂O, 59% N₂, 1 ppmv NaCl, 50 ppmv H₂S and 1000-2000 ppmw ash. The ash used to challenge the filters came from the Transport Reactor Demonstration Unit at University of North Dakota Energy and Environment Research Center. Some important results from the test campaign are summarized below.

- A data base was established on pressure drop of as-received filters as a function of face velocity and temperature. The observed pressure drop can be correlated with an effective permeability of $4.2 \pm 0.6 \text{ \AA}$. The data showed a visible trend of effective permeability increasing with gas temperature and face velocity. There was considerable filter to filter variation in effective permeability even though the specimens were from the same manufactured lot.
- On exposure, the effective permeability decreased to $2.9 \pm 0.5 \text{ \AA}$ over the temperature range 20-600°C. One effect of exposure to ash is to reduce the filter-to-filter variation in effective permeability measured with the as-received specimens. Post-test examination of the exposed filters revealed nearly uniform coating of the residual ash and a cake thickness of 0.5-1 mm.
- The mean collection efficiency of the filter, as-measured with a six-stage cascade impactor, is 99.92% for the challenge ash with a mass median aerodynamic diameter of 15.6 μm .
- A number of tests were conducted to investigate the effects of back pulse parameters on filter regenerability. At 600°C, a stable saw-tooth profile was established with a single 1-s pulse from a reservoir at 11.2 bar (150 psig). A saw-tooth profile was also observed at 7.8 bar (100 psig) reservoir pressure although the baseline pressure kept increasing slowly with time. A saw-tooth profile could not be established at 4.4 bar (50 psig) reservoir pressure. At 11.2 bar, a single pulse of 200 ms duration was also adequate in repetitively regenerating the filter to a stable baseline pressure. A double

pulse of 100 ms duration and 500 ms apart stabilized the filter at a slightly higher baseline pressure.

- The apparent bulk density of the filter, as measured by a geometrical method, was 0.293 g/cc for the virgin specimen and 0.387 g/cc after 3550 h of exposure. This trend of increase in bulk density with time of exposure was confirmed by mercury intrusion porosimetry data.
- The virgin filter has bimodal pore size distribution with 15% intrusion volume associated with submicron pores and >80% accounted for by pores in the 10-90 μm diameter range. Upon exposure, the cumulative intrusion volume decreased from 2.5 to 2.12 ± 0.12 cc/g and the median pore diameter from 40.3 to 23.9 ± 5.3 μm .
- The fast fracture strength of the filter specimens was measured with 0-ring compression tests. The load-displacement plots exhibit a composite material behavior. All specimens failed by debonding of the ceramic layers within the filter walls. The fast fracture strength increased from 401.3 ± 23 kPa for the virgin filter to 843.1 ± 30 kPa after 148 h, 1741.6 ± 10.8 kPa after 307 h, and 1819.2 ± 186.2 kPa after 3532 h.
- Based on the measured changes in bulk density, cumulative intrusion volume, median pore diameter and the fast fracture strength, it is suggested that the compliant VFCCF filter becomes rigidized upon exposure to the reducing environment containing H_2O vapor, trace amounts of NaCl and H_2S , and fly ash. This conclusion is corroborated by other indicators such as the measured deflection at peak load and the slope of the load-deflection curve.
- SEM and EDX analyses of the virgin filter indicate a composite material with a high fiber content. There is some knitting of fibers, somewhat random orientation of fibers, and the fiber diameter is $< 10\mu\text{m}$. One of the filter specimens showed a large amount of debris on both the inside and outside layers. During the experiment, this filter had proved difficult to regenerate. The EDX peaks were the same as those for the virgin filters indicating that there was no significant chemical attack during exposure. For the other filter specimens, ash particles were visible on the exposed outside surface but not on the inside surface.

ACKNOWLEDGMENTS

Research sponsored by the U.S. Department of Energy's Federal Energy Technology Center. Dr. Norman Holcombe was the FETC Contracting Officer's Representative. We thank Mr. Paul Eggerstedt of Industrial Filter & Pump Manufacturing Company for supplying the filter specimens and Dr. John Hurley of University of North Dakota for supplying the ash.

REFERENCES

1. Eggerstedt, P. M., "Lightweight Ceramic Filter Components: Evaluation and Application," Proceedings of the Advanced Coal-Fired Power Systems' 95 Review Meeting, Morgantown, WV, June 1995, Vol. 1, pp. 140-149.
2. Lee, S. H. D., Eggerstedt, P., and Zievers, J. F., "Preliminary Evaluation of the Fibrosic Candle Filter for Particulate Control in PFBC," Journal of the Institute of Energy, Vol. 9, June 1996, pp. 87-93.
3. Alvin, M. A., Lippert, T. E., Diaz, E. D., and Smeltzer, E. E., "Filter Component Assessment," Proceedings of the Advanced Coal-Fired Power Systems' 96 Review Meeting, Morgantown, WV, June 1996, DOE/METC-96/1037.
4. Swanson, M. L., and Ness, R. O., "Hot-Gas Filter Testing with a Transport Reactor Development Unit," Proceedings of the Advanced Coal-Fired Power Systems' 96 Review Meeting, Morgantown, WV, June 1996, DOE/METC-96/1037.
5. Swanson, M. L., personal communications, July 1998.